Materials Today Communications 29 (2021) 102865

Contents lists available at ScienceDirect

Materials Today Communications

journal homepage: www.elsevier.com/locate/mtcomm

Electrospinning of ternary composite of PMMA-PEG-SiO_2 nanoparticles: Comprehensive process optimization and electrospun properties

Mohammad Jafarpour [a,b], Araz Sheibani Aghdam [a,b], Ali Koşar [a,b,c], Fevzi Çakmak Cebeci [a,b], Morteza Ghorbani [a,c,d,*]

[a] Sabanci University Nanotechnology Research and Application Center, 34956 Tuzla, Istanbul, Turkey
[b] Faculty of Engineering and Natural Science, Sabanci University, 34956 Tuzla, Istanbul, Turkey
[c] Center of Excellence for Functional Surfaces and Interfaces for Nano-Diagnostics (EFSUN), Sabanci University, Orhanli, 34956 Tuzla, Istanbul, Turkey
[d] Department of Biomedical Engineering and Health Systems, KTH Royal Institute of Technology, SE-141 57 Stockholm, Sweden

ARTICLE INFO

Keywords:
Electrospun fibers
Membrane
Poly(methyl methacrylate)
Polyethylene glycol
Wettability

ABSTRACT

Electrospinning has been realized to be a promising method for creating nano-composite fibers due to its significant growth for producing innovative composites with advanced applications. In this method a polymeric solution subjected to an electrohydrodynamic process and slim charged liquid jet is formed inside a high potential electric field. The high voltage enables the production of continuously long fibers on a collector surface. Addition of different polymers and NPs to the one-component solution to modify the physicochemical characteristic and decorating the surface of electrospun fibers has proven to be challenging and imperative for many fields especially novel bioengineering and filtration applications. In this study, the effects of major parameters on the fabrication of electrospun fibers were extensively investigated. At the first step, formation of nanofibers on the surface of collector and optimization of process parameters were determined based on the mean diameter of resulting fibers, through SEM (Scanning Electron Microscopy) images. The optimum values for concentration, applied voltage, the distance between the tip of needle and collector, and flow rate determined to be 10 wt%, 12 kV, 20 cm, and 0.6 mL h^{-1}, respectively. Afterwards, the hydrophilicity of fibers was modified by adding different poly (ethylene glycol) (PEG) concentrations (20, 30, and 40 wt%) to the polymeric solution. The contact angle analysis revealed that the poly (methyl methacrylate) (PMMA) and 30 wt% PEG fabricated fibrous mat exhibited a better wettability and 71.61% lower hydrophobicity compared to pure PMMA electrospun mats. In the next step, silica NPs (nanoparticles) were introduced to the polymeric solution of electrospinning in the form of an IPA (isopropanol)-based collide solution. The dispersed solution-based addition of silica NPs prevented the aggregation state of NPs in the nanofibers. The addition of silica nanoparticles also changed the thermal and mechanical properties of the ternary composite, which were analyzed in TGA (thermogravimetric analysis) and tensile tests. Noteworthy, the addition of 30% PEG and silica NPs increase 3 times the tensile strength and around 2 times elongation in comparison with pure PMMA electrospun mats. These results highlight that the hybrid composite leads to a promising new electrospun mat for filtration and bioengineering applications.

1. Introduction

The development of nano-scale and advanced multifunctional composite materials has been a growing subject of interest in materials science [1]. Among the fabrication techniques, electrospinning has been rapidly emerging as a viable technique due to its simplicity, efficiency, low cost, and consistency in fabricating fibers, whose diameter could be reduced to tens of nanometers [2,3]. Electrospinning is an electrohydrodynamic process, where a high voltage is applied to generate a slim charged liquid jet followed by stretching the jet and solidifying continuously long fibers on a collector [4–6]. In general, the fabrication of electrospun fibers and control of their properties depend on several parameters, which can be divided into three main groups: electrospinning parameters (applied potential, flow rate of the solution, needle tip to collector distance, and needle diameter), solution properties concentration, polymer molecular weight, surface tension, etc.), and

* Correspondence to: Sabanci University Nanotechnology Research and Application Center, 34956 Tuzla, Istanbul, Turkey and KTH Royal Institute of Technology, SE-141 57 Stockholm, Sweden.
E-mail address: mortezag@kth.se (M. Ghorbani).

https://doi.org/10.1016/j.mtcomm.2021.102865
Received 28 June 2021; Received in revised form 24 September 2021; Accepted 30 September 2021
Available online 6 October 2021

ambient conditions [7,8].

The nonwoven structures with vast variety of materials have attracted great interest in various fields and applications, including filtration and wastewater treatment [9,10], biomedical and tissue engineering [11,12], sensors and catalysts [13,14], and energy storage [15,16] due to their high surface area to volume ratio, biocompatibility, porous networks, high permeability, and different types of surface morphology and modifications.

Poly(methyl methacrylate) (PMMA) a glassy and non-water-soluble polymer has been widely used in many fields. It possesses decent processing, biocompatibility, and inherent hydrophobicity [17,18]. However, the application of this material is constrained by its brittleness and low mechanical properties. Research efforts have been made to modify the fibers surface morphology and the influence of electrospinning parameters on the fiber properties [19]. For instance, Liu et al. [17] reported the solvent's effect on fabricated fiber morphology for water treatment application. Their study showed that the surface wettability of the PMMA fibers could be controlled by just adjusting the ratio of *N, N*-dimethylacetamide, and acetone in a binary solvent system. In one of the recent studies conducted by Li et al. [20], the experimental results exhibited an enhancement in the composite membranes' maximum adsorption capacity and mechanical strength with chitosan addition to PMMA.

To meet some application requirements, such as filtration and biomedical membranes, the mechanical properties and wettability of the electrospun mats should be adjusted [21,22]. The hydrophobic membranes usually cause clogging and flux-decline due to trapped air pockets within the mats. Thus, filters with a high-water contact angle are undesirable for filtration purposes [22,23]. The performance of the nanofibrous membranes could be improved by increasing the hydrophilicity of the fibers.

Blending a second component (polymer) is one of the most efficient and straightforward approaches for modulating the hydrophobicity of the fabricated membrane [24]. Poly(ethylene glycol) (PEG) is an ideal polymer to improve the wetting properties of nanofibers due to its hydrophilicity, solubility in water and organic solvents, and biocompatibility [4,24,25]. Kiani et al. [26] explained the effect of different PEG concentrations on the fabricated mat, whose characteristics such as water contact angle and tensile strength had great importance in the filtration applications. According to their results, incorporating 10 wt% of PEG in polyphenylsulfone enhanced the mechanical strength, decreased the water contact angle to 8.9°, and accordingly increased the water flux up to 7920 L/m^2 h.

Besides the wettability enhancements by mixing the PMMA with a second polymer, several studies were conducted to reveal the effects of adding nanoparticles such as TiO_2 [27], SiO_2 [28], Al_2O_3 [29], ZrO_2 [30], SiC [31], CNTs [32], and graphene [33] into the polymeric electrospun fibers. These nanoparticles were used to control the fibers' surface roughness and mechanical properties and improve their chemical properties by functionalizing the nanoparticles. An essential point to note is the nanoparticle dispersion uniformity in the polymeric electrospinning solution and fabricated composite mat [21].

SiO_2 nanoparticles (NPs) exhibit promising properties such as high mechanical strength, heat stability, chemical durability, and functionalizibility due to the presence of silanol groups in their structure [21, 34,35]. Moreover, the addition of mesopores and macropores silica NPs increases the surface roughness of fibers [36]. Although the addition of NPs could improve the tensile strength of the composite, the added amount should be optimized to prevent the decrease in the toughness and elongation of the mat at fracture strain [4]. Qing et al. [37] reported the development of Silica/PVA nanofibrous membranes for oil/water separation. They reported that silica NPs generated a multi-scale roughness on the PVA membrane and improved its wettability. The fabricated filters showed high wettability in the air and underwater superoleophobicity properties based on the successful strategy for surface modification. Multi-component materials based on the electrospinning process have been developed due to their enhanced properties, which could be promising to employ in a vast variety of fields such as bioengineering [38], filtration [39], and sensors [40]. Accordingly, the addition of different nanoparticles to the fibrous mat could improve the overall performance of the electrospun nanofibers, which cannot be achieved by single-component solutions.

The emerging studies on fabrications of a nanocomposite fibrous mat based on PMMA in DMF-based solutions suggest that blending the PMMA with PEG and adding colloid silica NPs in isopropyl alcohol (IPA) assist in modifying the surface of fibers as well as mechanical property improvements. These combinations of different characteristics of mentioned materials offer superior properties such as hydrophilicity, water insolubility, and higher mechanical strength to PMMA. In this study, the effects of electrospinning parameters and concentration of PMMA on the formation of electrospun fibers were systematically investigated. Also, surface wettability transition due to the addition of PEG besides the effect of silica NPs on the mechanical strength of the fibers was studied for potential applications such as gas filtration membranes. The gas filtration is mainly related to the existence of ether groups in the PEG chemical structure, which will be our future study on the performance of fabricated electrospun mats.

2. Materials and method

2.1. Chemicals and materials

Polymethyl methacrylate (PMMA, M_w = 350,000 g/mol), Poly (ethylene glycol) (average M_n ~ 400), N,N-Dimethylformamide (≥ 99%), Tetraethyl Orthosilicate (TEOS), Ammonia hydroxide solution 25%, and 2-Propanol (IPA, 99.5%) were purchased from Sigma Aldrich (technical grade) and were used without any purification.

2.2. Silica nanoparticles synthesis

Mesoporous silica nanoparticles were synthesized by the simple one-step synthesis modified Stöber method [41]. In this method, tetraethyl orthosilicate (TEOS) as the precursor was introduced to an alcoholic solution to be hydrolyzed with the water in the ammonia solution. The hydrolyzed precursors, which lost the EtOH groups on their structure, link together to create larger molecules and finally build up silica nanoparticles. In this study, five batches of synthesizing baths with [TEOS]/[NH3]aq ratios of 4, 4.8, 6, 8, and 12 were prepared to control the particle size of silica NPs.

2.3. Solution preparation and electrospinning

Solutions of PMMA in DMF with a polymer/solvent ratio of 10 and 12.5 w/w% were prepared and electrospun to investigate the effects of electrospinning parameters and polymer concentration on the surface coverage and fibers diameter. Electrospinning was conducted using a plastic syringe fitted with a metallic needle (inner diameter of the needle was 1 mm) at the accelerating voltages of 12–20 kV. The distance between the needle tip and fixed stainless-steel collector (11 × 11 cm^2) varied from 5 to 20 cm, and the flow rates were set in a range of 0.3–0.9 mL h^{-1}. After obtaining the optimum conditions for PMMA electrospinning and the best polymer/solvent ratio (10 wt%), three different polymer blends of PMMA-20 wt%, 30 wt%, and 40 wt% PEG with the fixed polymer/solvent ratio of 10 wt% were electrospun and characterized.

In the final step, silica NPs solutions (the synthesized method is explained in the next section) were added to electrospinning solution (with respect to fixed solid and powder: polymer ratios as 7.5 wt% and 10:90, respectively). All the electrospinning experiments were conducted at 22.7 °C and relative humidity of 48%. The prepared solutions were stirred overnight at 55 °C before the electrospinning process to obtain homogeneous solutions.

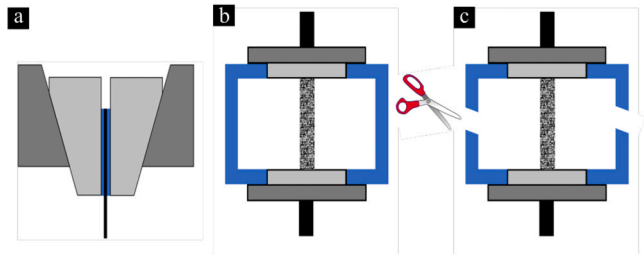

Fig. 1. Preparation of a frame before the tensile test. The samples were cut in 40 × 10 mm dimensions and sandwiched in a 40 × 40 mm paper frame a) the fibrous mat between a frame was held within grip, b) the system was stretched until the frame became ready to do the analysis, and c) the frame was cut to start the test.

2.4. Characterization

A double-shutter CMOS high-speed camera (Phantom v310, at 125 μs intervals (8000 fps)) along with a macro camera lens was employed to take images of the bending instability of the electrospun jets. The Field Emission Scanning Electron Microscopy (FE-SEM, LEO Supra VP-55) was used to evaluate the electrospun fibers and silica NPs morphology and size. The samples were sputter-coated with Au/Pd before imaging. Quantitative nanoscale mechanical (QNM) characterizations were performed using the Bruker MultiMode VIII Scanning Probe Microscope under ambient conditions at scan rates of 0.5–1 Hz. The spring constant of cantilever was measured as 25 N/m using the thermal tuning method [42] and the tip radius was measured as 17 nm. The Derjaguin–Muller–Toporov (DMT) modulus [43] was analyzed using the Nanoscope Analysis software. The surface coverage, fiber diameter, and size distribution of fibrous mats were determined using the ImageJ software (National Institutes of Health, MD, USA). The silica NPs size distribution was assessed by the Dynamic Light Scattering technique (DLS) using the Malvern Zetasizer Nano ZS device equipped with a He/Ne 633 nm laser light source. Thermal Gravimetric Analysis (TGA) was carried out by heating the samples with a rate of 10 °C/min from room temperature to 800 °C by the NETZSCH STA 449C instrument.

The chemical characterization of the fabricated composite fibers was performed using the Fourier transform infrared spectroscopy Nicolet iS10 spectrometer (Thermo Fisher Scientific Inc.) equipped with a universal attenuated total reflection (ATR) accessory. The samples were scanned from 500 to 4000 cm^{-1}. Dynamic contact angle measurements of deionized distilled water were conducted using the Attension Theta Lite. Samples were placed on the instrument's specimen holder, and a 5 μL droplet of water hanging from the tip of the needle was placed gently on the surface of the sample. The droplet's contact angle was observed using a video camera. The mechanical tests were performed using a Mark-10 ESM 303 motorized tension/compression test stand and M7–025 digital force gauge based on ASTM D882-10 standard test method for tensile properties of thin plastic sheeting with a thickness of less than 1 mm. The samples were cut in 40 × 10 mm dimensions and sandwiched in a 40 × 40 mm paper frame, as shown in Fig. 1. The paper frame was cut after fixing the sample in the grips, and then the test was performed at a strain rate of 5 mm/min.

3. Results and discussion

3.1. Fiber diameter and morphology

The effect of the parameters, namely solution concentration, accelerating voltage, flow rate, and the needle tip to collector distance, on the

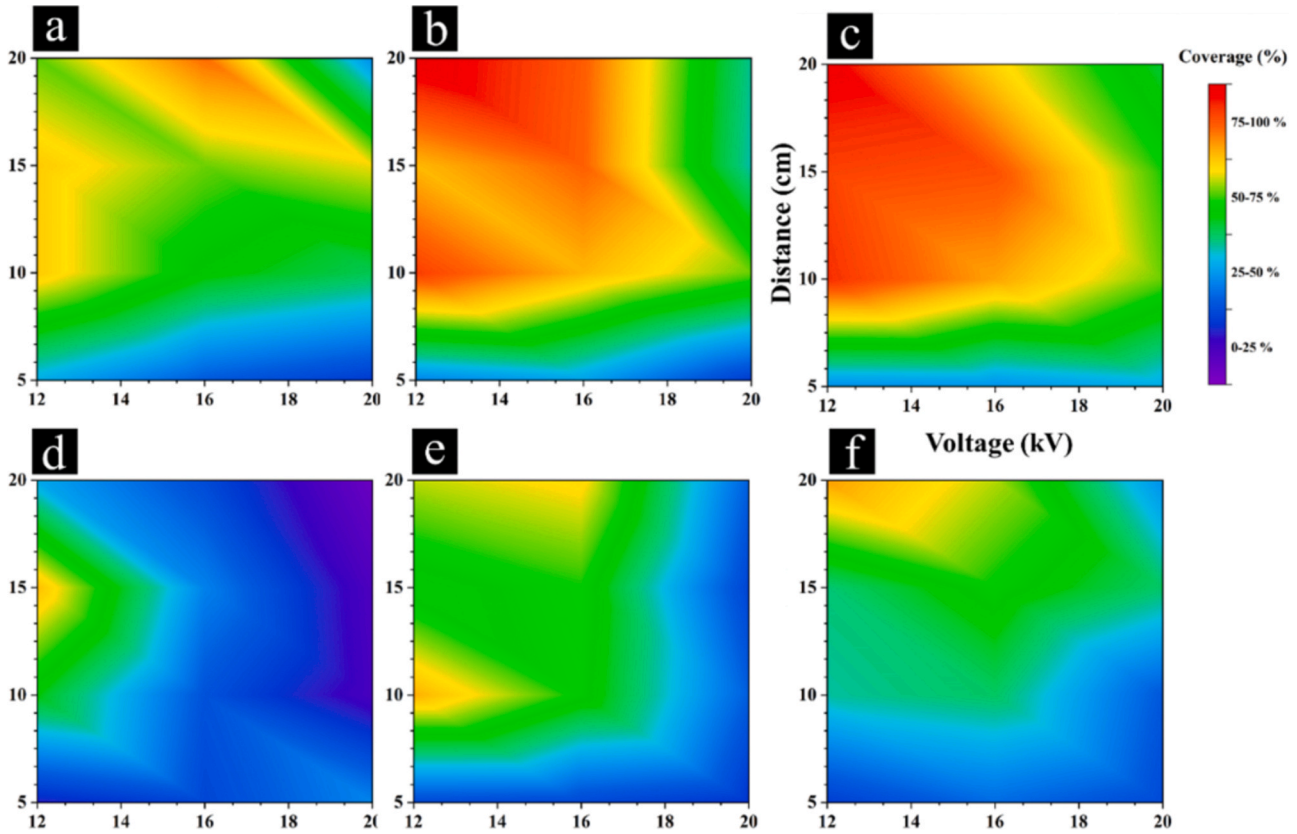

Fig. 2. Comparison of the formation fibrous mat of PMMA with different conditions of constant concentration and flow rate. a) C = 10 wt% and F.R. = 0.3 mL h^{-1}, b) C = 10 wt% and F.R. = 0.6 mL h^{-1}, c) C = 10 wt% and F.R. = 0.9 mL h^{-1}, d) C = 12.5 wt% and F.R. = 0.3 mL h^{-1}, e) C = 12.5 wt% and F.R. = 0.6 mL h^{-1}, and f) C = 12.5 wt% and F.R. = 0.9 mL h^{-1}.

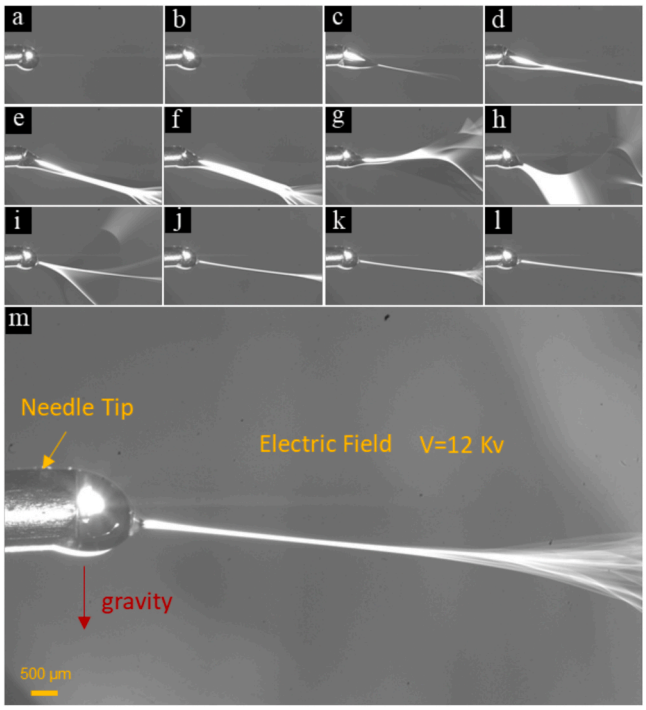

Fig. 3. Formation of the Taylor cone with process parameters of V = 12 kV, flow rate = 0.6 mL h^{-1}, distance = 20 cm, and composition = 10 wt% PMMA in DMF. (a and b) before applying the electric field, (c) the high-voltage and electric field cause stretching of the droplet toward the collector, (d–j) the instability of jet because of the interactions of the charges on the electrified microjet, (k–m) a stable slim microjet formation. The time intervals of the images are 6667 µs.

fibrous mat surface coverage and mean diameter of fibers are investigated by considering 72 different combinations of the parameters. Fig. 2 shows the surface coverage percentage of the electrospun fibers analyzed by the ImageJ software. In these diagrams, the optimum conditions for better coverage of the surface of the collector with nanofibers are shown with red color. Accordingly, the fiber mats cover less than 60% of the collector surface for the 12.5 wt% polymer/solvent solution. The polymeric solution viscosity increases with an increase in the concentration to 12.5 wt% polymer/solvent, which leads to a lower surface coverage. The low coverage could be explained by the higher viscoelastic force of the formed liquid jet, which resists the tension force during the electrospinning process [44]. The lower concentration (10 wt %) gives rise to the generation of a stable jet, and bead-free mats can be obtained besides other optimized parameters such as applied potential, distance, and flow rate. The electrospun fibers using this solution at the flow rates of 0.6 and 0.9 mL h^{-1} exhibit a sizeable red region (80–100% coverage) on their profiles. However, the flow rate of 0.3 mL h^{-1} was insufficient to provide enough material to cover the surface of the collector.

The electrospinning jet formation is visualized using a high-speed camera, as shown in Fig. 3. Prior to applying the high voltage between the needle tip and collector, the syringe pump injected the solution, and the shape of the droplet was distorted toward the ground due to the gravity force (Fig. 3a). The shape of the polymeric droplet, which emerges from the tip of the needle, is influenced by an electric field force and other forces such as inertia, hydrostatic pressure, and viscoelastic forces. By surpassing the electric field from the threshold point, the generated electrostatic charges on the droplet surface cause the elongation of the structure (so-called the Taylor cone). The forward electrostatic force and solution inertia overcome the backward viscous and downward gravity forces and form the jet (Fig. 3b, c). However, due to the droplet's rapid acceleration toward the collector and thick cross-section of the generated jet (Fig. 3d), the gravity force dominates and makes the unstable jet bend and move in different paths (Fig. 3e).

Meanwhile, the supplied amount of the solution is insufficient to provide enough material, and the Taylor cone becomes depleted (Fig. 3e, f). The unstable jet stabilizes by establishing a balance between the applied forces (Fig. 3g–i), and a continuous and stable electrospinning jet forms in 56 ms just after initiating the electrical field (Fig. 3j–m). During the stabilization stage, the multi-jet mode is visible for a fraction of a second, and the formed jets repel each other due to their identical charges which is shown in Fig. 3i (for more information with less intervals between images see ESI Figure S1).

The samples are shown in Fig. 2, which were electrospun uniformly, were selected to investigate the morphology and diameter of the fibers, and their SEM images and diameter distribution are included along with the corresponding label numbers in Fig. 4.

It is reported in the literature that the composite electrospun nanofibers with small diameters exhibit better mechanical properties and are more favorable for functionalization purposes due to the higher surface-to-volume ratio of the mat. Furthermore, in every case, well-defined and well-controlled (mostly narrow range) diameter distributions meet the requirements for optimizing the parameters [45].

The polymeric solution feeding rate directly affects the electrospun fiber morphology and formation of the beads during the process. The first stage is generally related to the charge density of the liquid cone and stable jet formation. It is also linked with the evaporation of solvent from polymeric fibers. The effect of feeding rate on the fiber diameter distribution can be observed in Fig. 4a–c, which displays that the size of fibers increases with the flow rate. Therefore, there should be a balance between the solution's feeding rate and the exiting material from the needle to obtain a continuous fiber with the smallest possible diameter. The solvent's evaporation takes place between the needle and collector, and the optimum distance provides sufficient time for the solvent to evaporate before reaching the collector. Otherwise, the formation of the beads would be inevitable. The longer the distance is, the thinner the fibers are. Based on the results as mentioned earlier, the electrospinning condition for obtaining fibrous mat from 10 wt% polymer/solvent solution with the fiber diameter of 696 nm and 100% surface coverage was optimized by applying the electric field of 12 kV, the flow rate of 0.6 mL h^{-1}, and the distance of 20 cm.

PEG was introduced to the solution as the second polymeric component. By considering 10 wt% polymer/solvent ratio as the optimum one for fabricating fibers, three solutions with PEG concentrations of 20, 30, and 40 wt% were electrospun, and the diameter of the obtained fibers are listed in Table 1. The mean fiber diameter decreases with the PEG concentration up to 30 wt%. The polymeric solution viscosity decreases by adding the low molecular weight PEG, and beads formation can be observed by electrospinning 40 wt% PEG solution. Moreover, the sufficient amount of the PEG does not interact with the PMMA solution to act as uniform compared to lower amounts.

The third component of the composite is the synthesized silica NPs in the IPA solution (Fig. 5). The different ratios of the TEOS to ammonia are taken as the control parameter for synthesizing different sizes of silica nanoparticles. The concentration of the synthesizing baths and the average size of the achieved silica nanoparticles are included in Table 2.

The third step of preparing a ternary electrospun composite is adding the silica nanoparticles to the PMMA-30 wt% PEG electrospinning solution. Synthesized silica NPs in different solutions in five levels were added to the solution with mentioned mean sizes. The solutions for hybrid material electrospinning were prepared considering the concentrations in Table 3.

The weights of silica NPs in each synthesized batch were different. Therefore, different solvent volumes (isopropyl alcohol) were used to prepare fixed concentration electrospinning solutions, as mentioned in Table 3. Since the ternary composite solution has different solvents, polymers, and other chemicals, the fabricated electrospun mats show different morphology, especially in the case of the formation of beads.

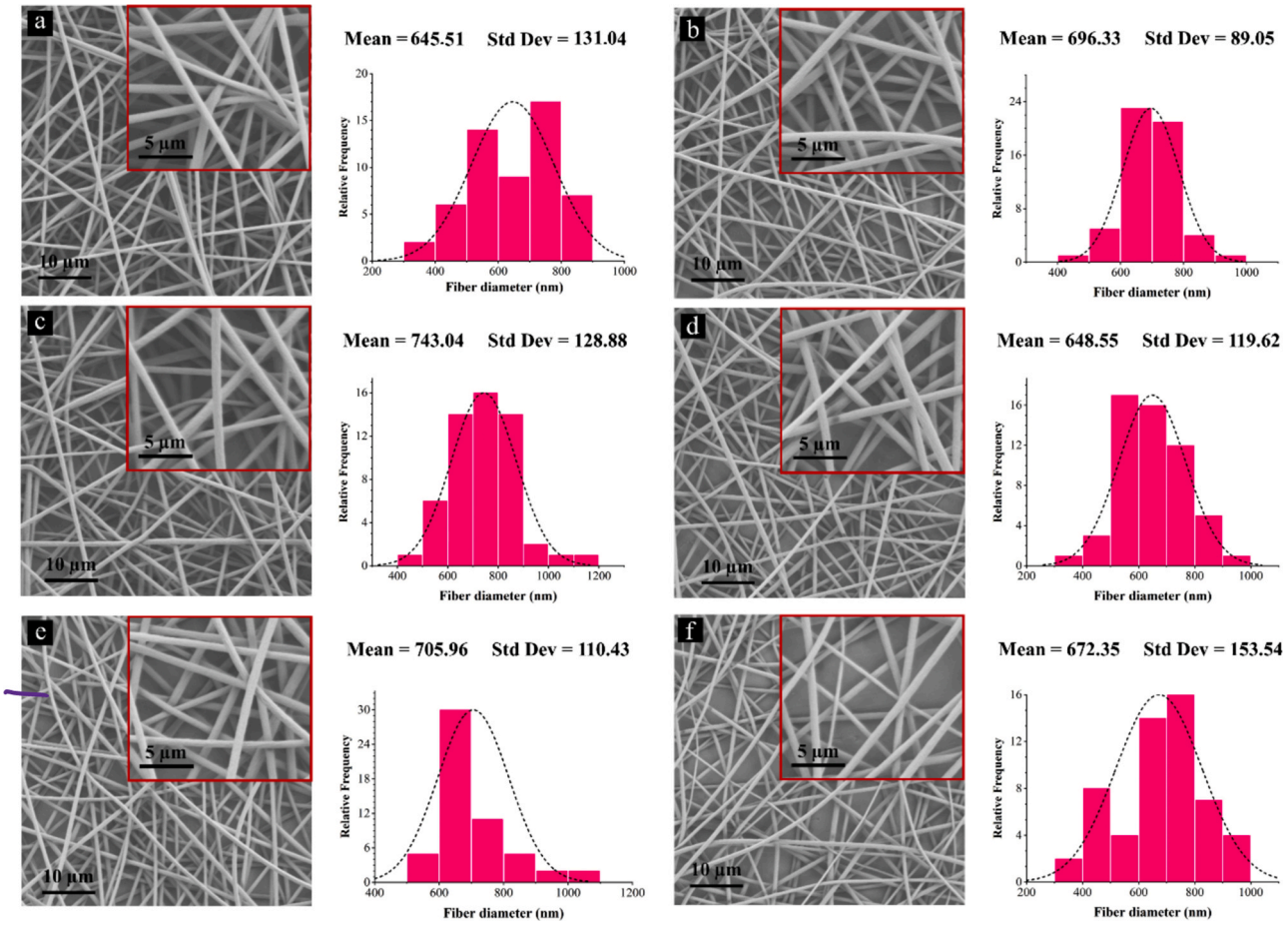

Fig. 4. SEM images and fiber diameter size distribution of PMMA electrospun mats for different process parameters. a) V = 12 kV, F.R. = 0.3 mL h^{-1}, and D = 10 cm, b) V = 12 kV, F.R. = 0.6 mL h^{-1}, and D = 20 cm, c) V = 12 kV, F.R. = 0.9 mL h^{-1}, and D = 10 cm, d) V = 12 kV, F.R. = 0.9 mL h^{-1}, and D = 15 cm, e) V = 12 kV, F.R. = 0.9 mL h^{-1}, and D = 20 cm, and f) V = 16 kV, F.R. = 0.9 mL h^{-1}, and D = 15 cm.

Table 1
The average diameter of electrospun PMMA nanofibers with the addition of different amounts of PEG.

Polymer solution composition	Nanofiber diameter (nm)
PMMA (Optimized Condition)	696.33 ± 89.05
PMMA-20 wt% PEG	472.75 ± 84.64
PMMA-30 wt% PEG	462.31 ± 89.91
PMMA-40 wt% PEG	747.65 ± 145.27

Table 2
Concentration of the baths and the sizes of the synthesized silica nanoparticles.

Batch number	$[TEOS]/[NH_3]_{aq}$	Mean particle size (nm)
1	4	102
2	4.8	97
3	6	86
4	8	74
5	12	65

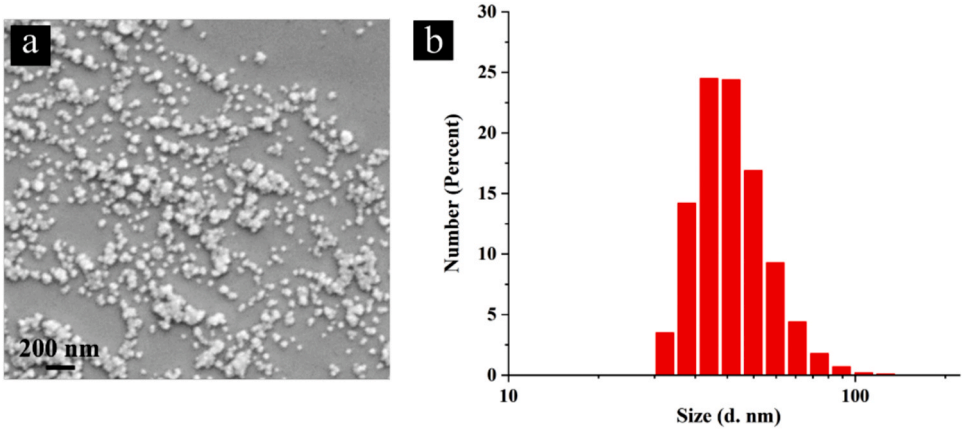

Fig. 5. Synthesized SiO_2 NPs a) SEM image of the particles after drying from the solution and b) particle size distribution of silica NPs in the synthesized medium.

Table 3
Concentrations of different materials and ratio of used materials concerning each other.

Parameter	Value
PMMA:PEG	70:30
Polymer solid ratio	10 wt%
Powder (SiO_2):Polymer	10:90
Solid (Polymer + SiO_2) Ratio	7.5 wt%

The first stage is related to the change in viscosity and then is linked with their conductivity and dipole-moment, volatile nature of the solvents, and evaporation of the solvents during the flight of polymeric fibers.

Fig. 6 shows the electrospun nanofibers with silica NPs on their surface for the optimum silica batch (batch number 5, Table 2). The optimum batch is achieved due to the lower alcohol amount, which transfers to the electrospinning solution from the synthesized silica batch. While silica NPs have an increasing effect on the viscosity, the inclusion of a second solvent (IPA) has an adverse effect. The balance between the counteracting effects results in batch 5, which leads to fewer beads in the electrospun mats.

3.2. PeakForce QNM

The nanoscale mechanical properties and surface of three samples of PMMA, PMMA-30 wt%PEG, and PMMA-30 wt%PEG-silica nanoparticles electrospun nanofibers are conducted (see ESI Figure S2). The height images and surface profile of the electrospun nanofibers (Fig. 7) show that the diameters of the fibers are in the range of 300 nm to 1 μm, which are consistent with the SEM images. The root mean square (RMS) of the DMT modulus of PMMA, PMMA-30 wt%PEG-silica nanoparticles, and PMMA-30 wt%PEG electrospun nanofibers are 126, 402, 441 MPa, respectively. The DMT modulus of PMMA-30 wt%PEG is the highest among the samples and these results are confirmed by the tensile strength tests. Fig. 8 shows PMMA-30 wt%PEG-silica nanoparticles electrospun nanofiber's height and DMT modulus profile. The AFM sample is prepared using scotch tape method by applying an adhesive

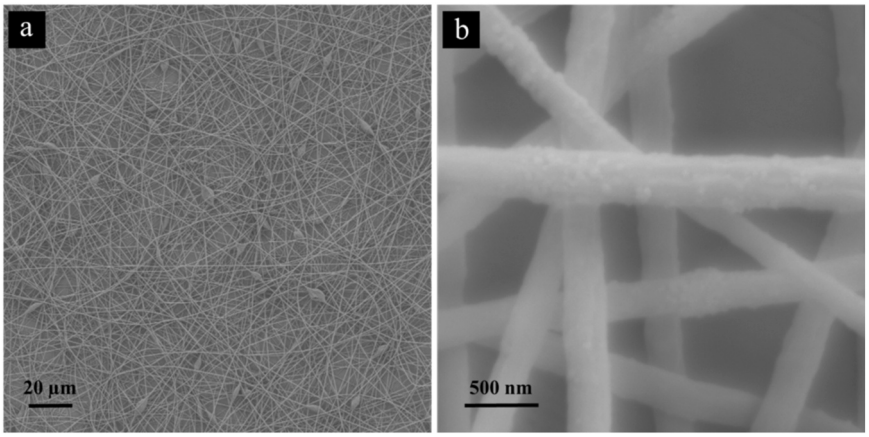

Fig. 6. SEM images of PMMA-30 wt% PEG-SiO_2 electrospun mats. a) The broad microscopic view with some beads, and b) homogenous distribution of silica NPs ascertained on the surface of fibers.

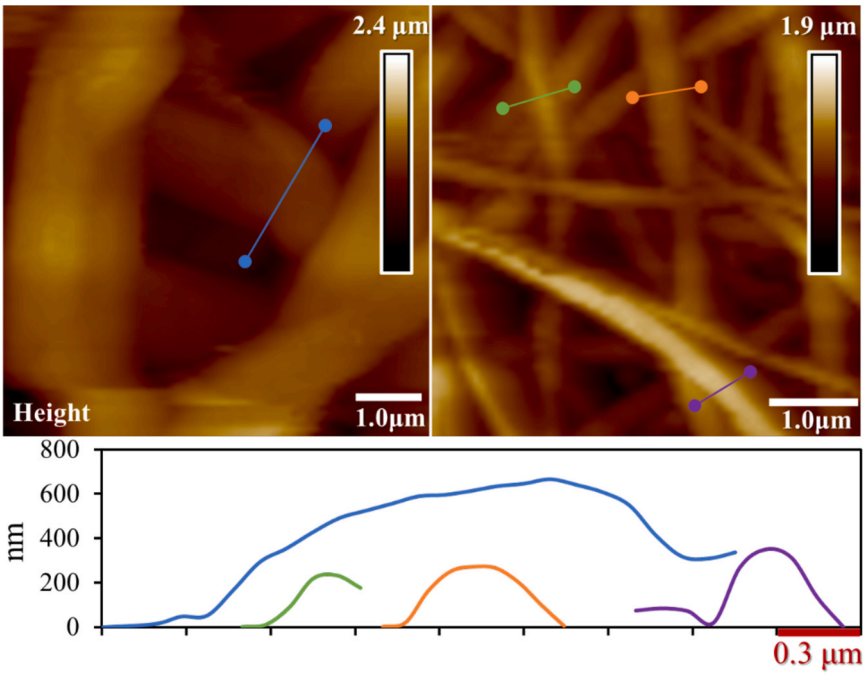

Fig. 7. AFM height images of PMMA electrospun nanofibers.

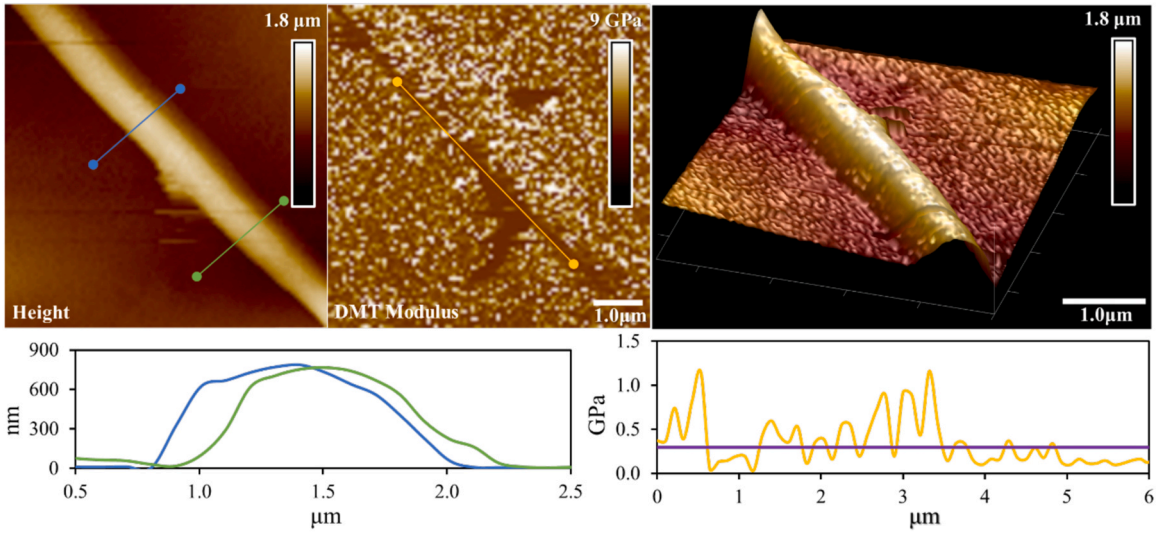

Fig. 8. AFM height image, DMT modulus, and 3D height image of PMMA-30 wt%PEG-silica nanoparticles electrospun nanofiber.

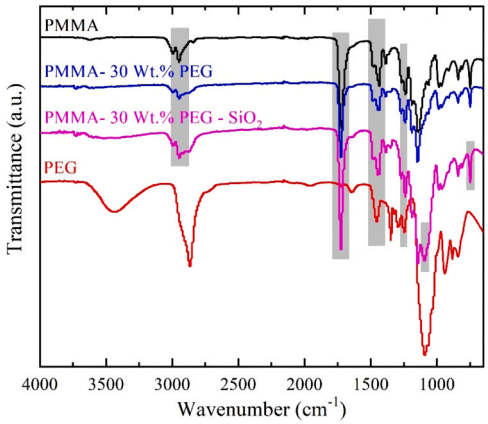

Fig. 9. FTIR spectra of PMMA, PEG, PMMA-30 wt% PEG electrospun mat, and PMMA-30 wt% PEG-SiO2 NPs electrospun mat.

tape to the electrospun nanofibers' mat and pulling it away and repeating the same procedure multiple times on the fresh adhesive tapes. The average DMT modulus of the electrospun fiber along its length is about 300 MPa. The observed picks on the DMT modulus diagram can be related to the silica nanoparticles, which are embedded in the structure of the fiber.

3.3. FTIR analysis

The FTIR analysis of the electrospun nanofibers is presented in Fig. 9. The peak at 2949 cm^{-1} is related to the C—H stretching vibration, and the peak at 1726 cm^{-1} corresponds to acrylate carboxyl groups. The FTIR band at 1386 cm^{-1} is due to O—CH_3 bending vibrations, whereas the peak at 1241 cm^{-1} is related to the twisting mode of the —CH_2 group in PMMA. The FTIR peak of PMMA at 1435 cm^{-1} stands for the bending of C—H bonds in the —CH_3 group, and the strong peak at 1147 cm^{-1} is associated with the stretching vibration of the C—O bond in the C—O—C moiety as shown in Fig. 9 [46,47]. For PEG, the 942–1092 cm^{-1} band originates from C—O ether groups stretching. The alkyl (R—CH_2) stretching modes at 2865 cm^{-1} can be observed, and the hydroxyl group contribution is observed at 3438 cm^{-1} [48]. The presence of SiO_2 can be confirmed with two main characteristic peaks at around 749 cm^{-1} and 1095 cm^{-1}, which correspond to Si—O bending vibration and asymmetric stretching vibration bands of the siloxane bonds (Si—O—Si), respectively. The band at around 3502 cm^{-1} is attributed to Si—OH, characteristics of the —OH group. The Si-OH band existence can be related to the absorbed water molecules from the environment by silica NPs [48].

3.4. Water contact angle

The water contact angle changes at 0, 5, and 10 s were measured to determine the effect of PEG content on the wettability of the PMMA-PEG electrospun (Fig. 10). PMMA is an intrinsic hydrophobic polymer [17], and the highest contact angle among the samples (123.52°) corresponds to the PMMA electrospun mat. Consequently, it shows low fouling, and flux and hydrophilicity improvements can be achieved by the addition of PEG due to easily linking repeating units (CH_2—CH_2O) with water molecules via hydrogen bonding. As shown in Fig. 10, the droplets start to diffuse inside the fibrous mats with different rates depending on the ratio of the blended polymer. The addition of the PEG up to 30 wt% shows a decrease in water contact angle (t = 0 s). However, in the PMMA-40 wt% PEG electrospun mat, an increase in water contact angle was observed. It seems that the solutions with a higher content of hydrophilic PEG lead to phase segregation of polymers and splashing PEG without any engagement in the morphology of fibrous electrospinning mats [49], which is in agreement with SEM images (see ESI Figure S3).

3.5. Thermal stability

The thermal stability of the electrospun mats was analyzed with TGA. The characteristic TGA curves of PMMA-based electrospun mats and the weight changes as a function of temperature for different electrospun fibers are compared in Fig. 11a. At the first stage, based on the hydrophobic properties of PMMA, just a tiny amount of weight loss can be seen at 0–100 °C. The second stage, between 250 and 300 °C, is related to the decomposition of PMMA unsaturated chain-ends. The third stage, above 300 °C (at around 365 °C), is attributed to the random scission of the polymeric chains [50]. The slight weight loss between room temperature to 100 °C, in Fig. 11b and c, results from the elimination of adsorbed water due to the hydrophobic nature of PMMA components. The weight loss steps in b and c are different and have higher losses since PEG was added to electrospun mats. For the cases, which contain PEG, at around 200 °C, the ether bonds (CH_2—O—CH_2) break and form more stable bonds of methylene (CH_2) and therefore, small molecules are released. At the range of 250–400 °C also, there is a degradation step for PEG and composite related to degradation and evaporation of the alcohol compounds (Fig. 11b) [51,52]. After the

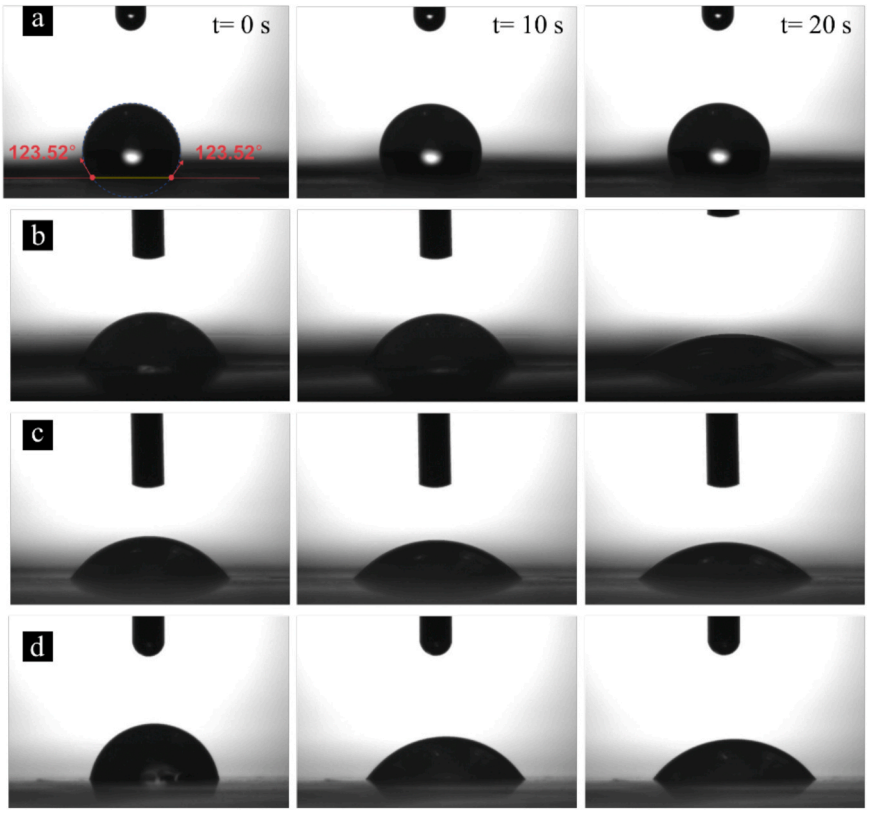

Fig. 10. Contact angle for a) PMMA, b) PMMA-20 wt% PEG, c) PMMA-30 wt% PEG and d) PMMA-40 wt% PEG at the beginning of analysis and after 10 and 20 s.

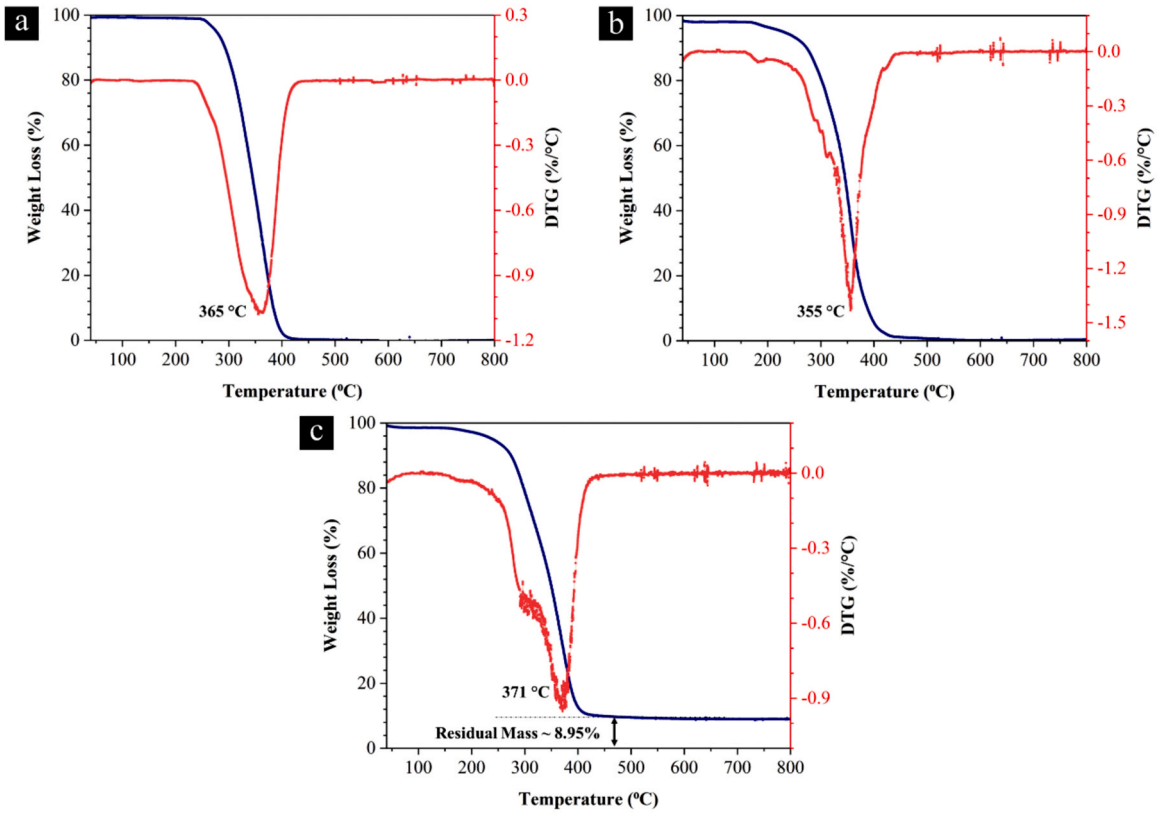

Fig. 11. TGA diagram of a) PMMA, b) PMMA-30 wt% PEG, and c) PMMA-30 wt% PEG-SiO_2 NPs electrospun mat.

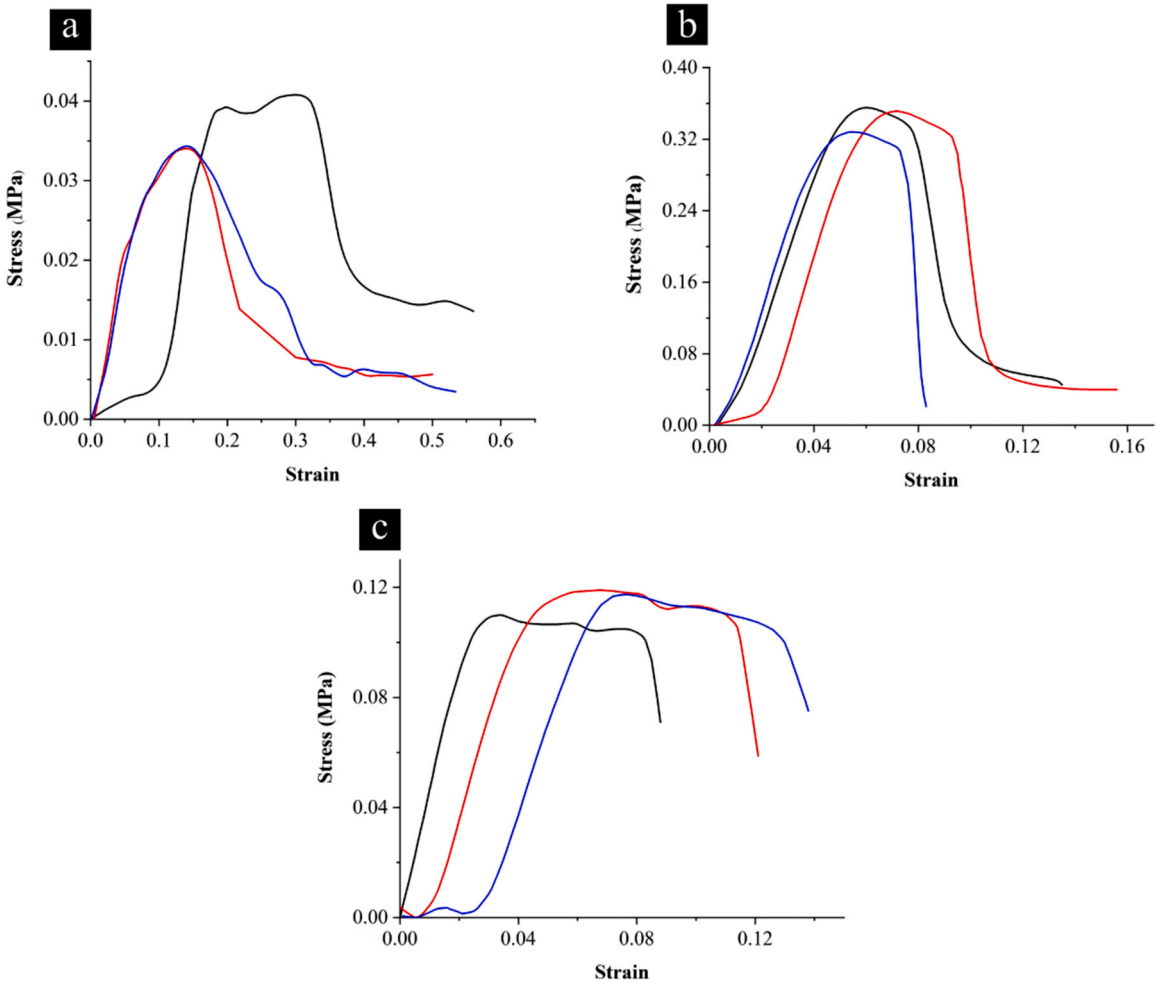

Fig. 12. Stress-strain curves of three different samples of a) PMMA b) PMMA-30 wt% PEG and c) PMMA-30 wt% PEG-silica NPs.

addition of silica NPs, the peak in the range of 270–330 °C is attributable to the release of silanol-bonded water since the silanol-bonded water is stable and is eliminated at relatively higher temperatures (Fig. 11c) [53]. At temperatures above 500 °C, the polymers decompose, and the entire polymer mass is burned. However, the embedded silica nanoparticles in the PMMA-30 wt% PEG-SiO_2 NPs do not decompose at temperatures above 500 °C. These results also prove that silica nanoparticles form almost 8% of the weight of the fibers.

3.6. Mechanical properties

For the applications such as filters and tissue engineering, the mechanical strength of electrospun mats is crucial for meeting the durability requirement. Therefore, the tensile tests were conducted to evaluate PMMA and PMMA-based composite electrospun nanofibers mechanical properties, and their stress-strain curves are given in Fig. 12. In some samples, the stress-strain curve has started with a lower slope, and then it has grown parallel to the other curves. It seems that in these samples, the fibers within the structure of the mat are loose and do not engage in the bearing of the applied load, and the stress makes them align with the direction of the force. The ultimate tensile stress and elongation at failure of the different electrospun mats are visible in this figure. The strength of polymeric materials can be improved with the addition of rigid reinforcement into the soft polymeric matrix, but this is accompanied by a compromise in ductility [54]. The ultimate strength of the samples is obtained as 0.035, 0.35, and 0.12 MPa for PMMA, PMMA-30 wt% PEG, and PMMA-30 wt% PEG-SiO_2 NPs, respectively.

Although the introduction of silica nanoparticles to the fibers reduces the mechanical properties of PMMA-PEG polymers, the functionalization and surface treatment could be performed more effectively in the presence of silica NPs. It should be noted that the PMMA-30 wt% PEG-silica nanoparticles have four times higher ultimate tensile strength in comparison with PMMA polymers.

4. Conclusion

In the present study, a PMMA-based electrospun nanofibrous composite was fabricated. The PMMA and PEG 400 blended solution in DMF was mixed with silica NPs solution in IPA to obtain a hybrid fibrous mat. Process parameters such as the applied voltage, distance of the needle tip to the collector, flow rate of solution and solution concentration were investigated. Based on fiber formation and covering of the surface of the collector, and mean fibers diameter, which is extracted from SEM images, the optimum parameters, namely concentration of PMMA, applied voltage, flow rate, and distance between needle tip to the collector, were achieved at 10 wt%, 12 kV, 0.6 mL h^{-1}, and 20 cm, respectively. Moreover, the Taylor cone formation was monitored under optimum conditions. Then, the influence of PEG concentration on altering the mean diameter of the fibers, hydrophobicity of electrospun mats, thermal and mechanical properties were studied. The results showed that blending and accordingly electrospinning of the PMMA solution with 30 wt% PEG led to improvements in wettability of electrospun mat.

Furthermore, the fabricated electrospun mats with PMMA-30 wt% PEG exhibited remarkable mechanical properties. The obtained ultimate

strength was around ten times larger than the pure PMMA. Moreover, the fabricated ternary composite of PMMA-30 wt% PEG-SiO_2 NPs led to three times enhancement in mechanical properties compared with PMMA, and the addition of silica NPs offers surface modification when needed in some applications such as filtration and bioengineering.

CRediT authorship contribution statement

Mohammad Jafarpour: Data curation, Formal analysis, Investigation, Validation, Visualization, Writing – original draft, Writing – review & editing. **Araz Sheibani Aghdam:** Conceptualization, Data curation, Formal analysis, Investigation, Methodology, Software, Validation, Visualization, Writing – original draft, Writing – review & editing. **Ali Koşar:** Validation, Writing – review & editing. **Fevzi Çakmak Cebeci:** Methodology, Writing – review & editing. **Morteza Ghorbani:** Conceptualization, Funding acquisition, Project administration, Resources, Supervision, Visualization, Writing – original draft, Writing – review & editing.

Declaration of Competing Interest

The authors declare that they have no conflict of interest.

Data availability

The data that support the findings of this study are available from the corresponding author upon reasonable request.

Acknowledgments

This work was supported by TUBITAK (The Scientific and Technological Research Council of Turkey) Support Program for Scientific and Technological Research Project Grant, 119M495. Equipment utilization support from the Sabanci University Nanotechnology Research and Applications Center (SUNUM) is gratefully appreciated. We thank Mr Vahid Charkhesht and Mr Ali Ansari for their helps regarding the electrospinning process.

Appendix A. Supporting information

Supplementary data associated with this article can be found in the online version at doi:10.1016/j.mtcomm.2021.102865.

References

[1] S. Ribeiro, T. Ribeiro, C. Ribeiro, D. Correia, J. Farinha, A. Gomes, C. Baleizão, S. Lanceros-Méndez, Multifunctional platform based on electroactive polymers and silica nanoparticles for tissue engineering applications, Nanomaterials 8 (2018) 933, https://doi.org/10.3390/nano8110933.
[2] J. Yoon, H.S. Yang, B.S. Lee, W.R. Yu, Recent progress in coaxial electrospinning: new parameters, various structures, and wide applications, Adv. Mater. 30 (2018), https://doi.org/10.1002/adma.201704765.
[3] X.X. He, J. Zheng, G.F. Yu, M.H. You, M. Yu, X. Ning, Y.Z. Long, Near-field electrospinning: progress and applications, J. Phys. Chem. C 121 (2017) 8663–8678, https://doi.org/10.1021/acs.jpcc.6b12783.
[4] F.E. Ahmed, B.S. Lalia, R. Hashaikeh, A review on electrospinning for membrane fabrication: challenges and applications, Desalination 356 (2015) 15–30, https://doi.org/10.1016/j.desal.2014.09.033.
[5] A.C. Mendes, K. Stephansen, I.S. Chronakis, Electrospinning of food proteins and polysaccharides, Food Hydrocoll. 68 (2017) 53–68, https://doi.org/10.1016/j.foodhyd.2016.10.022.
[6] J. Xue, T. Wu, Y. Dai, Y. Xia, Electrospinning and electrospun nanofibers: methods, materials, and applications, Chem. Rev. 119 (2019) 5298–5415, https://doi.org/10.1021/acs.chemrev.8b00593.
[7] A. Haider, S. Haider, I.K. Kang, A comprehensive review summarizing the effect of electrospinning parameters and potential applications of nanofibers in biomedical and biotechnology, Arab. J. Chem. 11 (2018) 1165–1188, https://doi.org/10.1016/j.arabjc.2015.11.015.
[8] M.S. Islam, B.C. Ang, A. Andriyana, A.M. Afifi, A review on fabrication of nanofibers via electrospinning and their applications, SN Appl. Sci. 1 (2019) 1–16, https://doi.org/10.1007/s42452-019-1288-4.
[9] M. Makaremi, R.T. De Silva, P. Pasbakhsh, Electrospun nanofibrous membranes of polyacrylonitrile/halloysite with superior water filtration ability, J. Phys. Chem. C 119 (2015) 7949–7958, https://doi.org/10.1021/acs.jpcc.5b00662.
[10] A.W. Lee, C.C. Hsu, C.J. Chang, C.H. Lu, J.K. Chen, Preparation of biofiltration membranes by coating electrospun polyacrylonitrile fiber membranes with layer-by-layer supermolecular polyelectrolyte films, Colloids Surf. B Biointerfaces 190 (2020), 110953, https://doi.org/10.1016/j.colsurfb.2020.110953.
[11] T. Wu, M. Ding, C. Shi, Y. Qiao, P. Wang, R. Qiao, X. Wang, J. Zhong, Resorbable polymer electrospun nanofibers: history, shapes and application for tissue engineering, Chin. Chem. Lett. 31 (2020) 617–625, https://doi.org/10.1016/j.cclet.2019.07.033.
[12] S. Ranganathan, K. Balagangadharan, N. Selvamurugan, Chitosan and gelatin-based electrospun fibers for bone tissue engineering, Int. J. Biol. Macromol. 133 (2019) 354–364, https://doi.org/10.1016/j.ijbiomac.2019.04.115.
[13] M.C. Li, S. Tong, J.T. Lin, K.Y.A. Lin, Y.F. Lin, Electrospun Co3O4 nanofiber as an efficient heterogeneous catalyst for activating peroxymonosulfate in water, J. Taiwan Inst. Chem. Eng. 106 (2020) 110–117, https://doi.org/10.1016/j.jtice.2019.10.010.
[14] S. Ulrich, S.O. Moura, Y. Diaz, M. Clerc, A.G. Guex, J.R. de Alaniz, A. Martins, N. M. Neves, M. Rottmar, R.M. Rossi, G. Fortunato, L.F. Boesel, Electrospun colourimetric sensors for detecting volatile amines, Sens. Actuators B Chem. 322 (2020), 128570, https://doi.org/10.1016/j.snb.2020.128570.
[15] L. Wang, Z. Wang, Y. Sun, X. Liang, H. Xiang, Sb2O3 modified PVDF-CTFE electrospun fibrous membrane as a safe lithium-ion battery separator, J. Membr. Sci. 572 (2019) 512–519, https://doi.org/10.1016/j.memsci.2018.11.041.
[16] X. Zheng, Y. Zheng, H. Zhang, Q. Yang, C. Xiong, Flexible MoS2@electrospun PVDF hybrid membrane as advanced anode for lithium storage, Chem. Eng. J. 370 (2019) 547–555, https://doi.org/10.1016/j.cej.2019.03.212.
[17] Z. Liu, J.H. Zhao, P. Liu, J.H. He, Tunable surface morphology of electrospun PMMA fiber using binary solvent, Appl. Surf. Sci. 364 (2016) 516–521, https://doi.org/10.1016/j.apsusc.2015.12.176.
[18] H.R. Munj, M.T. Nelson, P.S. Karandikar, J.J. Lannutti, D.L. Tomasko, Biocompatible electrospun polymer blends for biomedical applications, J. Biomed. Mater. Res. Part B Appl. Biomater. 102 (2014) 1517–1527, https://doi.org/10.1002/jbm.b.33132.
[19] S. Piperno, L. Lozzi, R. Rastelli, M. Passacantando, S. Santucci, PMMA nanofibers production by electrospinning, Appl. Surf. Sci. 252 (2006) 5583–5586, https://doi.org/10.1016/j.apsusc.2005.12.142.
[20] Z. Li, T. Li, L. An, P. Fu, C. Gao, Z. Zhang, Highly efficient chromium(VI) adsorption with nanofibrous filter paper prepared through electrospinning chitosan/polymethylmethacrylate composite, Carbohydr. Polym. 137 (2016) 119–126, https://doi.org/10.1016/j.carbpol.2015.10.059.
[21] T.E. Newsome, S.V. Olesik, Electrospinning silica/polyvinylpyrrolidone composite nanofibers, J. Appl. Polym. Sci. 131 (2014), https://doi.org/10.1002/app.40966.
[22] G. Moradi, S. Zinadini, L. Rajabi, S. Dadari, Fabrication of high flux and antifouling mixed matrix fumarate-alumoxane/PAN membranes via electrospinning for application in membrane bioreactors, Appl. Surf. Sci. 427 (2018) 830–842, https://doi.org/10.1016/j.apsusc.2017.09.039.
[23] M.S. Islam, J.R. McCutcheon, M.S. Rahaman, A high flux polyvinyl acetate-coated electrospun nylon 6/SiO2 composite microfiltration membrane for the separation of oil-in-water emulsion with improved antifouling performance, J. Membr. Sci. 537 (2017) 297–309, https://doi.org/10.1016/j.memsci.2017.05.019.
[24] E. Hendrick, M. Frey, Increasing surface hydrophilicity in poly(lactic acid) electrospun fibers by addition of Pla-b-Peg co-polymers, J. Eng. Fiber Fabr. 9 (2014), https://doi.org/10.1177/155892501400900219, 155892501400900.
[25] L.C. Lins, F. Wianny, S. Livi, I.A. Hidalgo, C. Dehay, J. Duchet-Rumeau, J.F. Gérard, Development of bioresorbable hydrophilic-hydrophobic electrospun scaffolds for neural tissue engineering, Biomacromolecules 17 (2016) 3172–3187, https://doi.org/10.1021/acs.biomac.6b00820.
[26] S. Kiani, S.M. Mousavi, N. Shahtahmassebi, E. Saljoughi, Hydrophilicity improvement in polyphenylsulfone nanofibrous filtration membranes through addition of polyethylene glycol, Appl. Surf. Sci. 359 (2015) 252–258, https://doi.org/10.1016/j.apsusc.2015.10.107.
[27] C. Kuchi, G.S. Harish, P.S. Reddy, Effect of polymer concentration, needle diameter and annealing temperature on TiO2-PVP composite nanofibers synthesized by electrospinning technique, Ceram. Int. 44 (2018) 5266–5272, https://doi.org/10.1016/j.ceramint.2017.12.138.
[28] Z.Q. Dong, X.H. Ma, Z.L. Xu, Z.Y. Gu, Superhydrophobic modification of PVDF-SiO2 electrospun nanofiber membranes for vacuum membrane distillation, RSC Adv. 5 (2015) 67962–67970, https://doi.org/10.1039/c5ra10575g.
[29] Z. Zhang, W. Zhang, M. Chen, Y. Jiang, R. Tian, J. Zhang, R. Fan, Fabrication of Co/Al2O3 composite nanofiber via electrospinning with tunable magnetic properties, Fibers Polym. 21 (2020) 2485–2493, https://doi.org/10.1007/s12221-020-1409-0.
[30] R. Sigwadi, T. Mokrani, S. Dhlamini, P.F. Msomi, Nafion® reinforced with polyacrylonitrile/ <scp> ZrO2 </scp> nanofibers for direct methanol fuel cell application, J. Appl. Polym. Sci. 138 (2021) 49978, https://doi.org/10.1002/app.49978.
[31] Y. Hou, L. Cheng, Y. Zhang, X. Du, Y. Zhao, Z. Yang, High temperature electromagnetic interference shielding of lightweight and flexible ZrC/SiC nanofiber mats, Chem. Eng. J. 404 (2021), 126521, https://doi.org/10.1016/j.cej.2020.126521.
[32] Y. Zhmayev, G.L. Shebert, S. Pinge, P. Kaur, H. Liu, Y.L. Joo, Non-enthalpic enhancement of spatial distribution and orientation of CNTs and GNRs in polymer nanofibers, Polymer 178 (2019), 121551, https://doi.org/10.1016/j.polymer.2019.121551 (Guildf.).

[33] E. Ceretti, P.S. Ginestra, M. Ghazinejad, A. Fiorentino, M. Madou, Electrospinning and characterization of polymer–graphene powder scaffolds, CIRP Ann. Manuf. Technol. 66 (2017) 233–236, https://doi.org/10.1016/j.cirp.2017.04.122.
[34] J. Seyfi, I. Hejazi, S.H. Jafari, H.A. Khonakdar, F. Simon, Enhanced hydrophobicity of polyurethane via non-solvent induced surface aggregation of silica nanoparticles, J. Colloid Interface Sci. 478 (2016) 117–126, https://doi.org/10.1016/j.jcis.2016.06.005.
[35] P. He, H.R. Cheng, Y. Le, J.F. Chen, Preparation and characterization of nano-sized Sr0.7Ca0.3TiO3 crystallines by low temperature aqueous synthesis method, Mater. Lett. 62 (2008) 2157–2160, https://doi.org/10.1016/j.matlet.2007.11.051.
[36] S. Sriram, A. Kumar, Separation of oil-water via porous PMMA/SiO2 nanoparticles superhydrophobic surface, Colloids Surf. A Physicochem. Eng. Asp. 563 (2019) 271–279, https://doi.org/10.1016/j.colsurfa.2018.12.017.
[37] W. Qing, X. Li, Y. Wu, S. Shao, H. Guo, Z. Yao, Y. Chen, W. Zhang, C.Y. Tang, In situ silica growth for superhydrophilic-underwater superoleophobic Silica/PVA nanofibrous membrane for gravity-driven oil-in-water emulsion separation, J. Membr. Sci. 612 (2020), 118476, https://doi.org/10.1016/j.memsci.2020.118476.
[38] Y. Chen, S. Liu, Z. Hou, P. Ma, D. Yang, C. Li, J. Lin, Multifunctional electrospinning composite fibers for orthotopic cancer treatment in vivo, Nano Res. 8 (2015) 1917–1931, https://doi.org/10.1007/s12274-014-0701-y.
[39] X. Yang, Y. Pu, Y. Zhang, X. Liu, J. Li, D. Yuan, X. Ning, Multifunctional composite membrane based on BaTiO3@PU/PSA nanofibers for high-efficiency PM2.5 removal, J. Hazard. Mater. 391 (2020), 122254, https://doi.org/10.1016/j.jhazmat.2020.122254.
[40] J. Zhang, H. Lu, C. Yan, Z. Yang, G. Zhu, J. Gao, F. Yin, C. Wang, Fabrication of conductive graphene oxide-WO3 composite nanofibers by electrospinning and their enhanced acetone gas sensing properties, Sens. Actuators B Chem. 264 (2018) 128–138, https://doi.org/10.1016/j.snb.2018.02.026.
[41] A.S. Aghdam, F.C. Cebeci, Tailoring the icephobic performance of slippery liquid-infused porous surfaces through the LBL method, Langmuir 36 (2020) 14145–14154, https://doi.org/10.1021/acs.langmuir.0c02873.
[42] R. Lévy, M. Maaloum, Measuring the spring constant of atomic force microscope cantilevers: thermal fluctuations and other methods, Nanotechnology 13 (2002) 33–37, https://doi.org/10.1088/0957-4484/13/1/307.
[43] B.V. Derjaguin, V.M. Muller, Y.P. Toporov, Effect of contact deformations on the adhesion of particles, J. Colloid Interface Sci. 53 (1975) 314–326, https://doi.org/10.1016/0021-9797(75)90018-1.
[44] E. Ghafari, Y. Feng, Y. Liu, I. Ferguson, N. Lu, Investigating process-structure relations of ZnO nanofiber via electrospinning method, Compos. Part B Eng. 116 (2017) 40–45, https://doi.org/10.1016/j.compositesb.2017.02.026.
[45] R. Stepanyan, A.V. Subbotin, L. Cuperus, P. Boonen, M. Dorschu, F. Oosterlinck, M. J.H. Bulters, Nanofiber diameter in electrospinning of polymer solutions: model and experiment, Polymer 97 (2016) 428–439, https://doi.org/10.1016/j.polymer.2016.05.045 (Guildf.).
[46] I.M. Joni, L. Nulhakim, M. Vanitha, C. Panatarani, Characteristics of crystalline silica (SiO2) particles prepared by simple solution method using sodium silicate (Na2SiO3) precursor, J. Phys. Conf. Ser. (2018) 12006, https://doi.org/10.1088/1742-6596/1080/1/012006.
[47] G. Soni, S. Srivastava, P. Soni, P. Kalotra, Y.K. Vijay, Optical, mechanical and structural properties of PMMA/SiO2 nanocomposite thin films, Mater. Res. Express 5 (2018) 15302, https://doi.org/10.1088/2053-1591/aaa0f7.
[48] H.S. Mansur, R.L. Oréfice, A.A.P. Mansur, Characterization of poly(vinyl alcohol)/poly(ethylene glycol) hydrogels and PVA-derived hybrids by small-angle X-ray scattering and FTIR spectroscopy, Polymer 45 (2004) 7193–7202, https://doi.org/10.1016/j.polymer.2004.08.036 (Guildf.).
[49] M. Spasova, O. Stoilova, N. Manolova, I. Rashkov, G. Altankov, Preparation of PLLA/PEG nanofibers by electrospinning and potential applications, J. Bioact. Compat. Polym. 22 (2007) 62–76, https://doi.org/10.1177/0883911506073570.
[50] S.R. Valandro, P.C. Lombardo, A.L. Poli, M.A. Horn, M.G. Neumann, C.C. S. Cavalheiro, Thermal properties of poly (methyl methacrylate)/organomodified montmorillonite nanocomposites obtained by in situ photopolymerization, Mater. Res. 17 (2014) 265–270, https://doi.org/10.1590/S1516-14392013005000173.
[51] M. Wang, A.J. Hsieh, G.C. Rutledge, Electrospinning of poly(MMA-co-MAA) copolymers and their layered silicate nanocomposites for improved thermal properties, Polymer 46 (2005) 3407–3418, https://doi.org/10.1016/j.polymer.2005.02.099 (Guildf.).
[52] T. Qian, J. Li, W. Feng, H. Nian, Enhanced thermal conductivity of form-stable phase change composite with single-walled carbon nanotubes for thermal energy storage, Sci. Rep. 7 (2017) 1–10, https://doi.org/10.1038/srep44710.
[53] X.M. Hu, D.M. Wang, W.M. Cheng, G. Zhou, Effect of polyethylene glycol on the mechanical property, microstructure, thermal stability, and flame resistance of phenol-urea-formaldehyde foams, J. Mater. Sci. 49 (2014) 1556–1565, https://doi.org/10.1007/s10853-013-7838-z.
[54] R. Scaffaro, F. Lopresti, A. Maio, L. Botta, S. Rigogliuso, G. Ghersi, Electrospun PCL/GO-g-PEG structures: processing-morphology-properties relationships, Compos. Part A Appl. Sci. Manuf. 92 (2017) 97–107, https://doi.org/10.1016/j.compositesa.2016.11.005.